Improved Forecasts of the Diurnal Cycle in the Tropics Using Multiple Global Models. Part II: Asian Summer Monsoon

ARINDAM CHAKRABORTY AND T. N. KRISHNAMURTI

Department of Meteorology, The Florida State University, Tallahassee, Florida

(Manuscript received 18 June 2007, in final form 11 March 2008)

ABSTRACT

The diurnal mode of the Asian summer monsoon during active and break periods is studied using four versions of the Florida State University (FSU) global spectral model (GSM). These versions differ in the formulation of cloud parameterization schemes in the model. Observational-based estimates show that there exists a divergent circulation at 200 hPa over the Asian monsoon region in the diurnal time scale that peaks at 1200 local solar time (LST) during break monsoon and at 1800 LST during active monsoon. A circulation in the opposite direction is seen near the surface. This circulation loop is completed by vertical ascending/descending motion over the monsoon domain and its surroundings. This study shows that global models have large phase and amplitude errors for the 200-hPa velocity potential and vertical pressure velocity over the monsoon region and its surroundings. Construction of a multimodel superensemble could reduce these errors substantially out to five days in advance. This was on account of assigning differential weights to the member models based on their past performance. This study also uses a unified cloud parameterization scheme that inherits the idea of a multimodel superensemble for combining member model forecasts. The advantage of this model is that it is an integrated part of the GSM and thus can improve the forecasts of other parameters as well through improved cloud cover. It was seen that this scheme had a larger impact on forecasting the diurnal cycle of cloud cover and precipitation of the Asian summer monsoon compared to circulation. The authors show that the diurnal circulation contributes to about 10% of the rate of change of total kinetic energy of the monsoon. Therefore, forecasting this pronounced diurnal mode has important implications for the energetics of the Asian summer monsoon.

1. Introduction

The diurnal cycle contributes to a large modulation of the time-mean energy budget of the earth–atmosphere system. Bergman and Salby (1997), from radiative transfer calculations, showed that large errors can occur in the estimation of TOA (a list of acronyms is provided in Table 1) shortwave ($\sim$20 W m^{-2}) and longwave fluxes ($\sim$5 W m^{-2}) if the diurnal cycle is not taken into account. Chakraborty et al. (2007) showed that improvements in the diurnal cycle of low, middle, and high cloud covers in a GCM can indeed result in an improvement of the TOA shortwave and longwave fluxes of the same order. Improved diurnal variation of radiative fluxes in a model can have an impact on the diurnal variation of surface wind and divergence (Dai and Deser 1999), precipitation (Krishnamurti et al. 2007), and water cycle (Trenberth et al. 2003).

Krishnamurti and Kishtawal (2000) reported a continental-scale divergent circulation gyre over the Asian summer monsoon region in the diurnal time scale. Both wind and precipitation (TRMM) datasets were used to confirm the presence of this diurnal swing of convection and the related divergent wind. This day–night swing of the divergent gyre has a lateral scale of several thousand kilometers and appears to be a prominent scale of the Asian summer monsoon. The ascent of warmer air in the daytime over the continent and descent over the surrounding oceans (with a reverse scenario occupying the nighttime) raises the possibility of a steady exchange of energy from the diurnal scale to the scale of the Asian summer monsoon. Modeling of this gyre and its implications for the behavior of the monsoon are some of the unsolved problems. This has motivated us to extend the previous study.

Temperature, cloudiness, convection, and circulation have a phase-locked relationship in the diurnal time

Corresponding author address: Arindam Chakraborty, Dept. of Meteorology, The Florida State University, Tallahassee, FL 32306.
E-mail: arch@io.met.fsu.edu

DOI: 10.1175/2008JCLI2107.1

TABLE 1. List of acronyms used in this paper.

CAPE	Convective available potential energy
CC	Correlation coefficient
CCM3	Community Climate Model, version 3
ECMWF	European Centre for Medium-Range Weather Forecasts
FSU	The Florida State University
GCM	General circulation model
GSM	Global spectral model
IR	Infrared
ISCCP	International Satellite Cloud Climatology Project
LST	Local solar time
NCAR	National Center for Atmospheric Research
PC	Pattern correlation
PBL	Planetary boundary layer
SST	Sea surface temperature
TOA	Top of the atmosphere
TRMM	Tropical Rainfall Measuring Mission

scale (Tian et al. 2004; Dai 2001; Randall et al. 1991). Tian et al. (2004) have shown that the phase of high clouds follows the phase of convective precipitation over both land and oceans. The phases, however, show wide variations over different parts of the tropics (Shin et al. 1990; Janowiak et al. 2005; Yang and Smith 2006). In general, precipitation over land (oceans) shows an afternoon (early morning) maximum (e.g., Dai 2001). This is primarily due to the fact that the thermal capacity of land is less compared to the ocean. Therefore, land is heated up faster by solar radiation in daytime. This leads to destabilization of the atmosphere through increase in CAPE (Dai 2001) and results in showery precipitation over land. Deep convection, in turn, has a direct impact on the vertical motion of the atmosphere (Randall et al. 1991). Therefore, cloud cover, precipitation, and circulation are interrelated for their diurnal phase selection.

The TRMM dataset provided a unique opportunity for the mapping of the diurnal change of rainfall over the global tropics. Yang and Smith (2006) have described the phase and amplitude of tropical rainfall covering all of the seasons. They have shown that spatial variability of the diurnal change of rainfall is quite large and is not a simple contrast of early morning rains over the tropical oceans and the late afternoon showers over the land areas of the tropics. Krishnamurti et al. (2007) and Chakraborty et al. (2007) had demonstrated the out of phase relationship of precipitation and high clouds within a small spatial scale over the eastern Tibetan Plateau and the eastern foothills of the Himalayas.

The coherent temporal and geographical variations of the diurnal mode of convection, cloudiness, and circulation makes it a good test bed for the validation of numerical model forecasts (Yang and Slingo 2001; Dai and Trenberth 2004). In this study we address the issue of modeling the diurnal mode of the Asian summer monsoon. This is a sequel to two recent papers on diurnal change of precipitation and cloudiness over the tropics (Krishnamurti et al. 2007; Chakraborty et al. 2007). In those two studies we examined the impacts of different cloud radiation transfer algorithms on the distribution of the phase and amplitude of diurnal change. These studies found that major improvements in the modeling of the diurnal change in distribution of cloudiness and precipitation over the global tropics is possible from the construction of a multimodel superensemble (Krishnamurti et al. 1999). Further, construction of a new statistical–physical-based unified cloud parameterization scheme (Chakraborty et al. 2007) that used the notion of a multimodel superensemble could also substantially reduce the errors in the diurnal cycle of clouds and precipitation. This resulted in an improved radiation budget at the TOA from a single model framework.

The next section outlines the numerical model and describes the cloud parameterization schemes used. Section 3 provides in detail the processing of ISCCP DX1 pixel datasets for the construction of the unified cloud scheme and validation of cloud diurnal cycle results. Section 4 mentions the experiments performed. The unified cloud parameterization scheme is described in section 5. Section 6 illustrates the results in detail. The main findings of this study are summarized in section 7.

2. Model used

The FSU GSM was used in this study to construct ensemble forecasts with four different cloud schemes. The horizontal resolution of the model had a triangular truncation at 126 waves (T126), which corresponds to roughly 0.94° grid separation in both latitude and longitude directions. The model had 27 vertical sigma levels with more closely spaced levels near the surface and at the tropopause. The main features of the model are given in Krishnamurti et al. (2007).

Four versions of the model differ in the use of four different cloud parameterization schemes. All other components of the model were kept unchanged between different members of the ensemble. The main features of these schemes are provided below.

a. FSUnew cloud parameterization

Clouds can form at any layer of the model in this parameterization scheme. A threshold relative humid-

TABLE 2. Threshold relative humidity for three different cloud types of the FSUnew scheme.

Cloud type	RH_c
High	0.40
Middle	0.45
Low	0.70

TABLE 3. Threshold relative humidity for three different cloud types of the FSUold scheme.

Cloud type	α	RH_c
High	1.67	0.40
Middle	2.00	0.45
Low	2.94	0.66

ity, which varies with cloud height, determines the presence of cloud in a layer. If the mass-weighted relative humidity in a model layer exceeds the threshold relative humidity, then the cloud fraction in that layer is calculated from the following relation:

$$CC = \left(\frac{RH - RH_c}{1 - RH_c}\right)^2, \quad (1)$$

where RH is the mass-weighted relative humidity of that layer and RH_c is the threshold relative humidity. Table 2 lists the values for RH_c for three different cloud types used in this model. This scheme also corrects the high cloud fraction from the information of convective precipitation amount using the following relation when the precipitation rate (P, mm) is nonzero:

$$CC_h = 4(0.247 + 0.126\ln P - 0.3)^2. \quad (2)$$

b. FSUold cloud parameterization

Similar to the FSUnew scheme, this scheme also used threshold relative humidity criteria to calculate cloud fraction in a model layer. However, FSUold differs from the FSUnew in the formulation of high clouds. FSUold did not implement the correction of the amount of high clouds from convective precipitation criteria. Moreover, FSUold used a different equation for the calculation of cloud fraction when relative humidity crosses the threshold

$$CC = [\alpha(RH - RH_c)]^2, \quad (3)$$

where α is a proportionality factor, RH_c is the threshold relative humidity, and RH is the mass-weighted relative humidity in that layer. Table 3 provides the values of α and RH_c used by this parameterization scheme for three different could types.

c. NCAR–CCM3 cloud parameterization

This cloud parameterization scheme is adapted from NCAR–CCM3 model. This scheme is based on Slingo (1987) and used large-scale parameters, such as relative humidity and vertical stability, to calculate cloud fraction. Convective cloudiness is calculated from the mean convective motion in an atmospheric column. Stability of the atmospheric column is considered to be the criterion for determining the presence of layered clouds. Low clouds are allowed to present only if the vertical velocity is less than 50 hPa day^{-1}. Relative humidity criteria determine the presence of clouds associated with the low-level inversion.

d. Pleim–Xiu cloud parameterization

This parameterization scheme is based on Pleim and Xiu (1995) that, similar to the other three parameterization schemes, used relative humidity criteria for the calculation of cloud fraction. However, unlike other schemes, in this model the threshold relative humidity is a function of pressure of the layer:

$$RH_c = 1 - 2\frac{P}{P_s}\left(1 - \frac{P}{P_s}\right)\left[1 - \sqrt{3}\left(\frac{P}{P_s} - 0.5\right)\right], \quad (4)$$

where P is pressure of the layer and P_s is surface pressure. In addition to that, in the nonconvective planetary boundary layer, the maximum relative humidity threshold is set to 0.90. Cloud fraction in a layer is derived from the mass-weighted relative humidity in that layer using Eq. (1), where the threshold relative humidity RH_c is derived from Eq. (4).

All of these schemes used large-scale parameters such as relative humidity, pressure, vertical stability, and CAPE to calculate cloud fraction diagnostically from large-scale parameters. Originally we intended to include a prognostic cloud scheme in our suite of models. The advantage of a prognostic cloud scheme is that it includes and predicts (as dependent variables) cloud fraction and the liquid water mixing ratio (e.g., Sundqvist 1978; Sundqvist et al. 1989); hence, there is a direct effect of cloud fraction on the convection and circulation in the model. However, in Krishnamurti et al. (2007) and Chakraborty et al. (2007) we have seen that large improvement can come for the modeling and forecasting of the diurnal change of different cloud types, radiation budget, and precipitation from the use of these simple diagnostic cloud schemes. Thus, we limited this study to the use of a suite of diagnostic cloud schemes.

3. ISCCP datasets

Construction of the unified cloud schemes and validation of the results related to the cloud diurnal cycle in

this study used ISCCP DX1 pixel datasets (Rossow and Schiffer 1999). During our study period (May–August 2000), data from 5 geostationary satellites and 16 polar-orbiting satellites were available that covered the globe. The spatial resolution of the DX1 pixels is 30 km × 30 km and time resolution is 3 h. ISCCP DX1 datasets provided a binary flag that declared a pixel to be either clear or cloudy separately for both visible and IR wavelengths. The visible threshold results covered only daylight hours, whereas the IR threshold results include both day and night hours. Earlier studies (Rossow et al. 1993; Rozendaal et al. 1995) show that there can be considerable difference in the cloud fractions using only the IR thresholds versus those from the visible adjusted IR (VIS/IR) thresholds. Since in this study we are concerned about the diurnal cycle of cloud cover, which requires data of similar characteristics both during day and night, we used only the IR threshold results to estimate the cloud fractions. The mean was removed prior to calculation of the diurnal cycle: therefore, bias in the IR data that possibly arises from algorithm or instrumental problem (a possible constant bias during day and night) might have canceled out when the IR data was used both during the day and the nighttime.

In the hierarchy of satellites, geostationary satellites got higher preference than polar-orbiting satellites when data from both of them were available on a grid. We adopted a very similar processing technique that was used to produce the ISCCP equal-area (280 km) cloud fractions from DX1 pixels (described in the ISCCP cloud dataset user's guide).

Finally, the pixel data were mapped to the model grid (~0.94° in the FSU GSM) to obtain cloud fraction at different heights. Cloud fraction in a model grid was calculated by dividing the total area of cloudy pixels by the area of that grid. Cloud-top pressure of the cloudy pixel was used to classify cloud types according to their height (low clouds can exist below 700 hPa, middle clouds between 700–400 hPa, and high clouds above 400 hPa). We did not make any overlapping assumption to calculate low, middle, and high cloud fractions from ISCCP satellites. This process provided global equal-angle-gridded 3-hourly cloud fractions from ISCCP satellite-based estimates. A detailed description of this cloud processing algorithm is provided in Chakraborty et al. (2007).

4. Experiments, periods of study, and validation datasets

We have chosen the boreal summer monsoon season of the year 2000 for this study: the choice of this year was rather arbitrary. One set of forecasts for each of the four member models was made for every initial condition starting at 1200 UTC 1 May to 31 August 2000. Therefore, there were 123 forecast experiments altogether for every member of the ensemble. The length of each forecast was 5 days. Initial conditions were taken from the 40-yr ECMWF Re-Analysis (ERA-40). Weekly mean SSTs from Reynolds and Smith (1994) were prescribed over ocean after interpolation to the model run time.

Outputs of the model were obtained at 3-hourly intervals (at 0000, 0300, . . . , 2100 UTC) for estimating the diurnal cycle. For studying the diurnal cycle of velocity potential and circulation we have used only the 0000, 0600, 1200, and 1800 UTC forecasts because the ERA-40 dataset, which was used for forecast verification, was available at those time points. A study of the diurnal cycle of clouds and precipitation used all of the eight 3-hourly forecasts. Starting at 1500 UTC (or 1800 UTC for winds) on the day of the model start to 1200 UTC the next day, all forecast times together were designated as day-1 forecasts in this study; day-2 through day-5 forecasts follow similarly. A time series of the day n ($n = 1, 2, \ldots, 5$) forecasts were created by joining the string of day n forecasts from 123 separate forecasts for each member of the ensemble.

The superensemble forecast of day n was constructed from the time series of day-n forecasts of the member models. The 123 days of the day-n forecasts were divided into a training phase and a forecast phase. The first 76 days were taken as the training period and the last 47 days as the forecast period in this study. It was found that for an adequate length of training datasets ($\geq$75 days) (Mishra and Krishnamurti 2007) the weights become stabilized. A set of separate statistical weights was calculated for every output hour of the day by regressing the forecasts valid at that hour against corresponding observations (3-hourly ISCCP datasets for cloud covers, 3-hourly TRMM datasets for precipitation, and 6-hourly ERA-40 datasets for winds and temperature). This exercise resulted in 20 different sets of weights for the winds and temperature (6-hourly) and 40 different sets of weights for clouds and precipitation (3-hourly), one for every lead time and at every 3 or 6 h of the day from day 1 to day 5 of the forecasts. The assignment of separate weights for different lead times was necessary to account for any change in the characteristics of the models with an increase in the forecast lead time. The day-n superensemble forecast was made from the day-n weights obtained from the above procedure.

The four forecasts of winds and temperature and eight forecasts of clouds and precipitation in a day were used to obtain the diurnal cycle through a Fourier

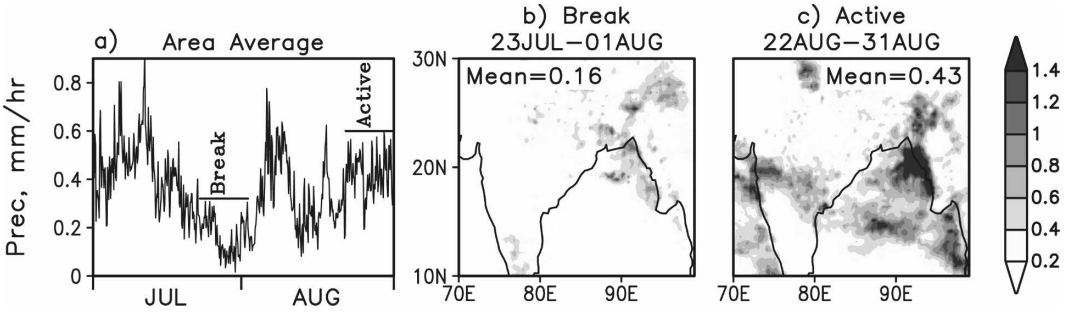

FIG. 1. (a) Area-averaged precipitation (mm h^{-1}) from TRMM over 10°–30°N, 70°–100°E during July–August 2000: period of study is from 23 Jul to 1 Aug for break monsoon and from 22 to 31 Aug for active monsoon. Mean precipitation during the (b) break monsoon period (area average = 0.16) and (c) active monsoon period (area average = 0.43).

transform. The first harmonic of the transformed time series is defined as the diurnal cycle in this study. An hour-by-hour composite of all forecast days constructs the mean diurnal cycle during that period.

Figure 1a shows the time series of 3-hourly precipitation from TRMM 3B42 datasets over the South Asian monsoon region (10°–30°N, 70°–100°E) during July and August of 2000. There were three active (or wet) spells separated by two break (or dry) spells of monsoon over this region during this period. To do a complete study of the diurnal cycle of the Asian monsoon, we selected two 10-day-long periods: one characterized with low precipitation (23 July to 1 August: break period) and the other with high precipitation (22–31 August: active period). The spatial distribution of the mean precipitation over the two 10-day periods is shown in Figs. 1b,c. The area-averaged precipitation values over the region during the break and active periods were 0.16 and 0.43 mm h^{-1}, respectively. This large difference in precipitation is characteristic of the two opposite phases of the South Asian monsoon.

We have used different datasets for validating relevant forecast parameters in this study: ERA-40 6-hourly datasets were used for winds and temperature, ISCCP 3-hourly satellite-based estimates for cloud fractions, and TRMM 3-hourly estimates (Kummerow et al. 2000) for precipitation. In the following parts of this paper we will refer to these datasets as observational truths.

5. The unified cloud parameterization scheme

A unified scheme for cloud parameterization was developed by Chakraborty et al. (2007). This scheme used the notion of the superensemble (Krishnamurti et al. 1999, 2000) to make consensus forecasts from all member parameterization models. Part I of this study describes the superensemble methodology in detail (Krishnamurti et al. 2008). Here, the timeline of the available dataset is divided into two parts: a training period and a forecast period. The model forecasts are regressed in the training period with the ISCCP estimates. The outcome of this regression is the weights assigned to the models. These weights are then passed on to the forecast phase to make the superensemble forecast using the following equation:

$$S = \overline{O} + \sum_{i=1}^{N} a_i(F_i - \overline{F}_i), \tag{5}$$

where $\overline{O}$ is the observed climatology and a_i is the weight for the ith member in the ensemble; F_i and $\overline{F}_i$ are the forecasts and forecast climatological values for the ith model's forecast, respectively. The summation is taken over the N member models of the ensemble. The weights a_i are obtained by minimizing an error term. This exercise was performed for every grid point and vertical level in the dataset during every forecast lead time. In other words, one weight is given to every model at every grid point in the three-dimensional space for each (3- or 6-h interval) forecast. It is the selection of these differential weights that make the superensemble perform better than bias-removed ensemble mean forecasts (Stefanova and Krishnamurti 2002; Chakraborty and Krishnamurti 2006). It has been shown by Stefanova and Krishnamurti (2002) that the superensemble algorithm can also be used to make an equivalent probabilistic forecast.

This idea of a superensemble was first extended to construct a unified scheme by (Krishnamurti and Sanjay 2003) from a collection of member cumulus convection parameterization schemes. It was shown in Chakraborty et al. (2007) that a unified cloud parameterization scheme performed better than the individual member models in predicting the diurnal cycle

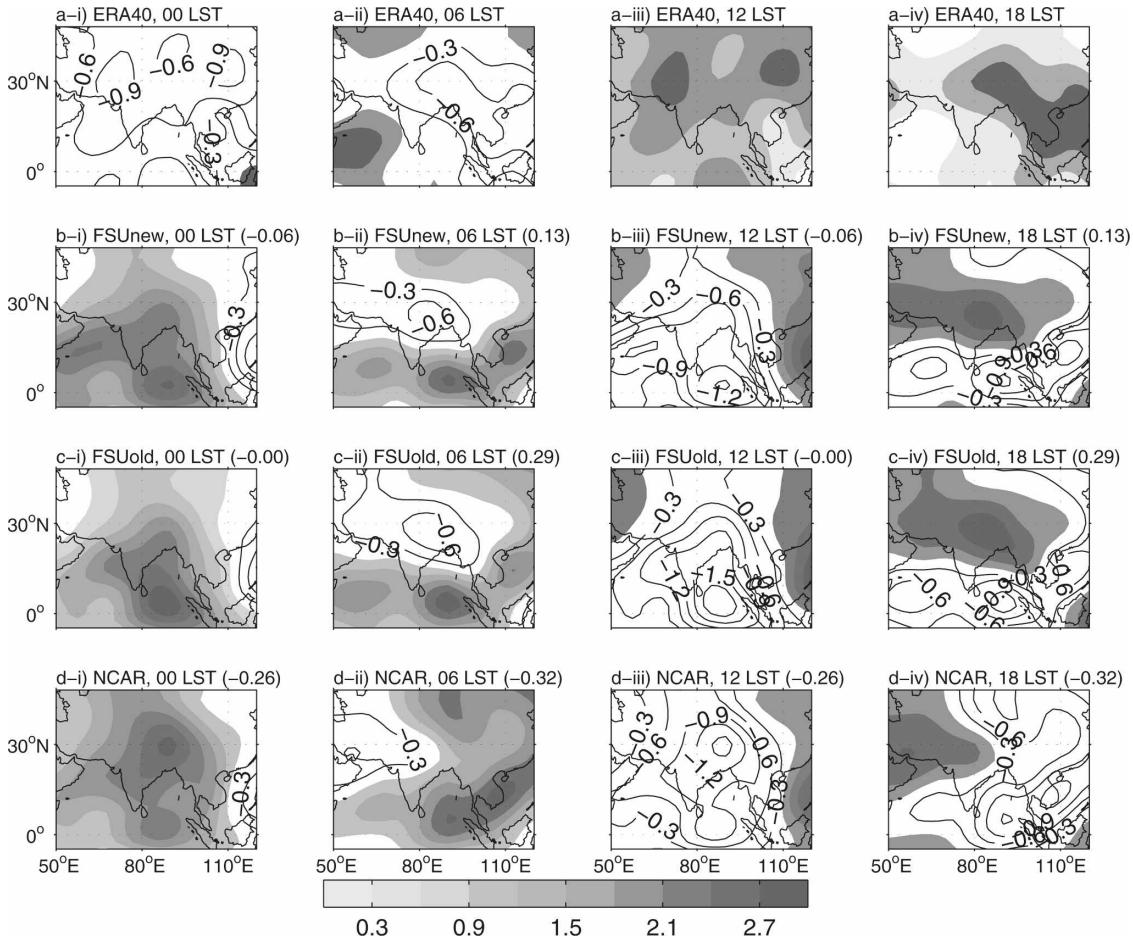

FIG. 2. The diurnal cycle of velocity potential (10^6 m^2 s^{-1}) at 200 hPa from ERA-40, and day 3 of the forecasts of four member models, their ensemble mean, the unified cloud scheme, and the superensemble during 23 Jul to 1 Aug 2000 (break monsoon season): pattern correlation of the forecasts with the observed fields indicated as numbers at the top of the panels within parentheses.

for different types of cloud cover. The direct impact of this improvement was the enhanced skill in forecasting the TOA radiation budget.

In the unified cloud parameterization scheme, all four member cloud schemes were run in parallel in a single model to obtain four sets of cloud forecasts at every radiation time step of the model. These forecasts were then combined using the respective weights of the models. The weights of the models were obtained from the superensemble methodology. The training period was taken from 1 May to 15 July 2000. These weights varied geographically. Moreover, different weights were obtained for low, middle, and high cloud types. Since the bias of a model can vary with lead time in the forecast, we have calculated superensemble weights for each of the 3-h intervals of a forecast during a day and at each forecast lead time. These weights for different cloud fractions were then applied to the cloud forecasts from four member models to construct a single consensus unified forecast. This is the forecast of the unified cloud scheme. These forecasted cloud fractions were then used by the other parts of the model (e.g., shortwave and longwave radiation calculations) and interacted fully as the forecast evolved. Chakraborty et al. (2007) described the methodology of the unified cloud parameterization scheme in detail.

The unified cloud parameterization scheme statistically combines the cloud forecasts of physically based parameterization models based on their past performance. This scheme was flexible in terms of the number of models in the ensemble, and any number of input member models can, in principle, be used to construct the unified scheme. It was shown by Krishnamurti et al. (2003) and Chakraborty and Krishnamurti (2006) that a superensemble forecast scheme improves if better models are used in the suite. Thus, including better cloud

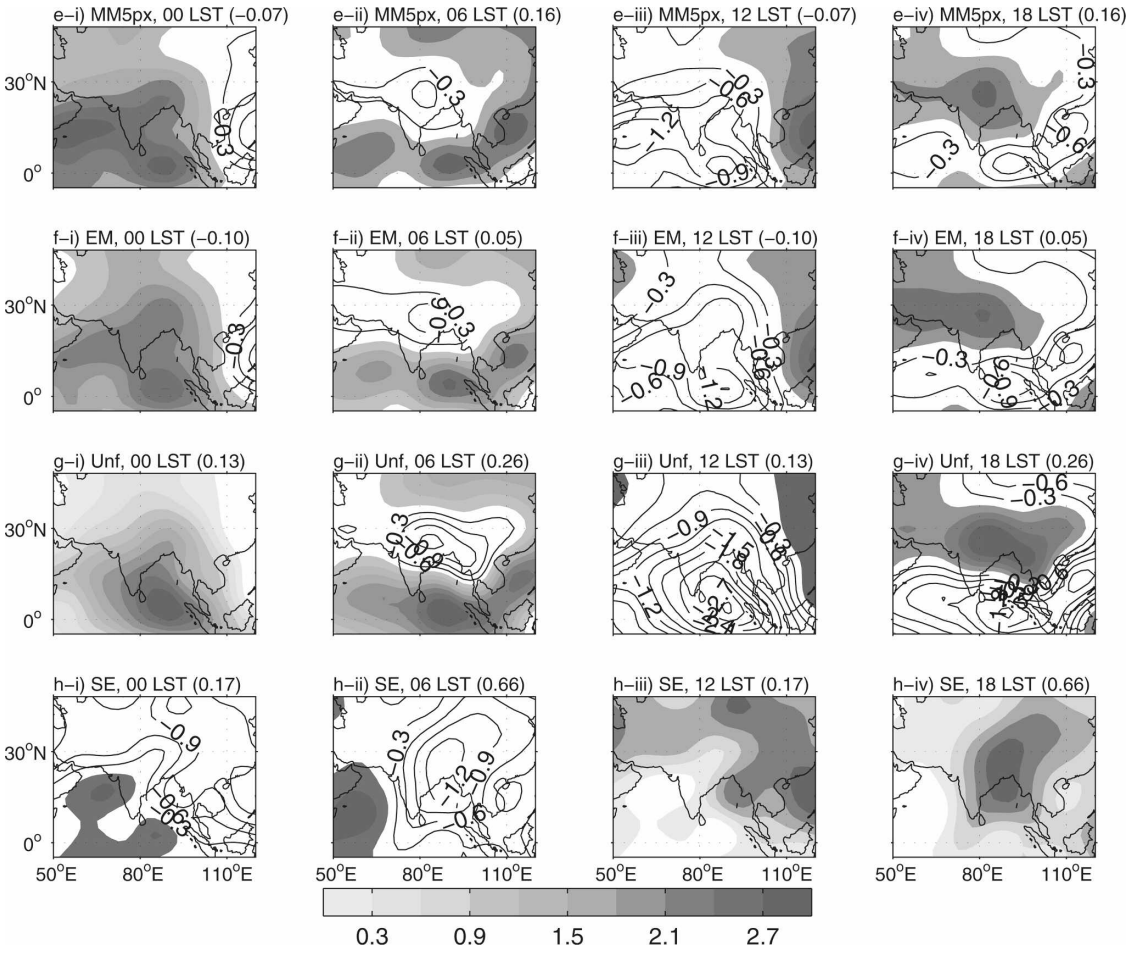

FIG. 2. (*Continued*)

schemes (e.g., a prognostic scheme) in the suite of models can enhance the skill of the unified cloud parameterization scheme.

6. Results

a. Diurnal cycle of velocity potential

The diurnal cycle of velocity potential for the divergent component of winds at 200 hPa from ERA-40 datasets, and day 3 of forecasts of the four member models, their ensemble mean, the unified cloud scheme, and the superensemble are shown in Figs. 2 and 3 for the break and active monsoon periods, respectively. Also shown, at the top of the forecast panels within parentheses, is the pattern correlation (PC) of the forecasted fields to that of ERA-40. A spatial gradient in velocity potential signifies wind flow from its high value region to the low value region:

$$\mathbf{V}_h = -\nabla_h \chi, \tag{6}$$

where $\mathbf{V}_h$ is the horizontal wind vector, ∇_h the horizontal gradient operator, and χ the velocity potential. In the ERA-40 data for the break monsoon [Figs. 2a(i) to 2a(iv)] a relative negative (compared to its surroundings) velocity potential is noticed over the South Asian monsoon region during 0000 and 0600 LST. This negative velocity potential peaks at 0600 LST over the northeastern parts of India with the diurnal magnitude of $\sim 10^6$ m^2 s^{-1}. During this time the value of velocity potential over the Arabian Sea and equatorial Indian Ocean is positive. This signifies a wind flow into the South Asian monsoon region from its surroundings at this pressure level. The situation reverses during 1200 and 1800 LST. Figures 2b–f show that the member models failed to forecast the phase, magnitude, and location of the high and low of velocity potential fields over this region. For example, at 1800 LST, all four models and their ensemble mean show a peak in velocity potential over the northwestern part of South Asia where a heat low prevails. This is in contrast to the

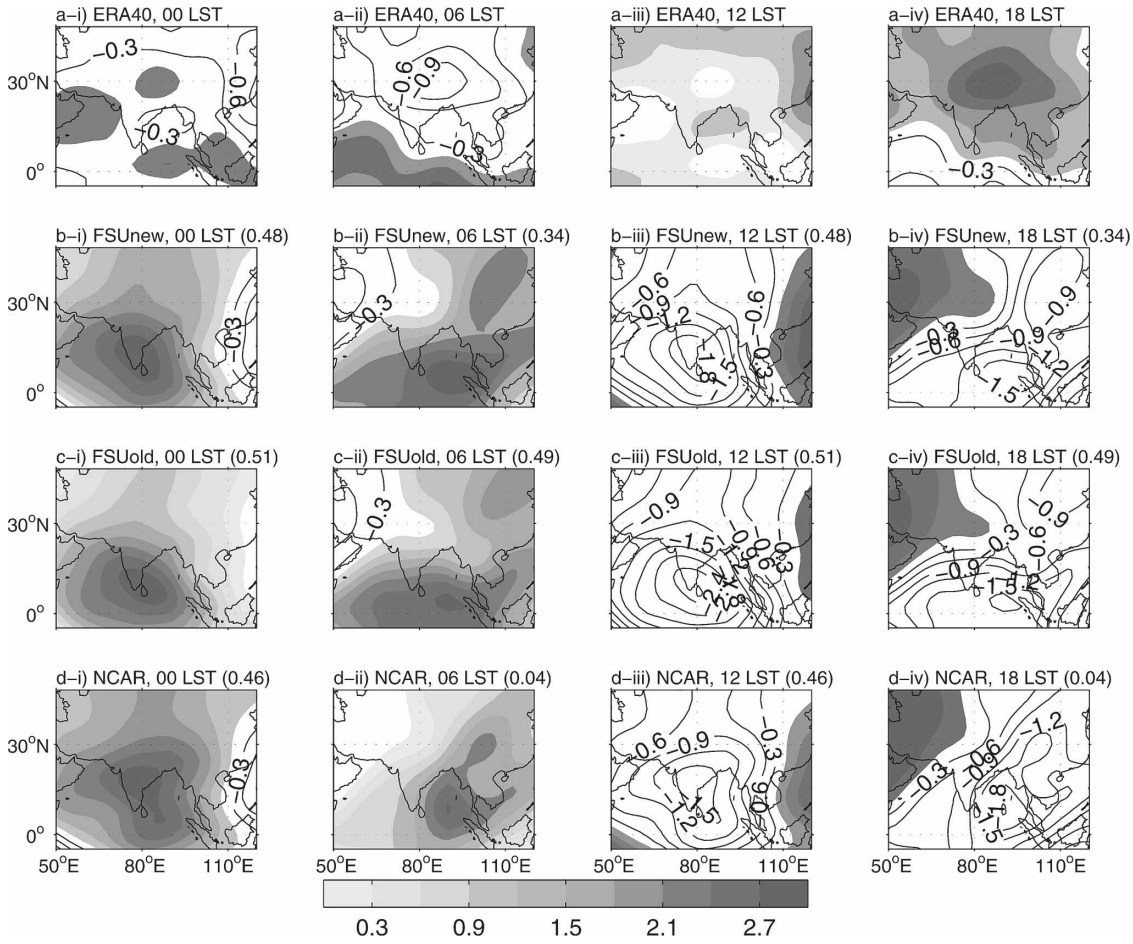

FIG. 3. As in Fig. 2 but during the 22–31 Aug 2000 active monsoon season.

observed high over northeast India where a monsoonal low is situated during this time of the year. The PC of most of the models and their ensemble mean with the observed counterpart is poor (ranges from −0.32 to 0.29). For the unified cloud scheme (Fig. 2g), the main improvement over the member models is noticed over the northeast Indian region where low (high) velocity potential during 0600 (1800) LST was successfully forecasted. Figure 2h shows that a superensemble could reasonably well predict the location and intensity of this diurnally varying high and low of velocity potential. The signature of a dipolelike structure with a minimum (maximum) over northeast India and a maximum (minimum) over the equatorial Indian Ocean at 0600 (1800) LST is present in this forecasts. The PCs for the superensemble and the unified scheme are higher compared to those of the member models and their ensemble mean during 0600 and 1800 LST.

During the active monsoon period (Fig. 3), the peak of the velocity potential over the Asian monsoon region occurs at 1800 LST, compared to 1200 LST for the break monsoon period (Figs. 2a and 3a, respectively). None of the member models show high skill in forecasting this phase of velocity potential at 200 hPa. In fact, all of these models and their ensemble mean show the peak at 0000 and 0600 LST, suggesting 6 to 12 h of phase error. The PC of the forecasted fields has improved with use of the unified scheme, but large phase errors remain over many regions during all four time slots of the day. It was possible to attain the highest PC with the superensemble forecast during 1800 LST (Fig. 3h) when the velocity potential reaches its peak. Comparing Figs. 3a and 3h we find that high values of velocity potential over the South Asian landmass are best captured by the superensemble methodology.

The above results show that there exists a diurnal mode of the 200-hPa velocity potential of the Asian summer monsoon in both the ERA-40 data and the model forecasts. At midnight and during early morning hours (0000 and 0600 LST) the velocity potential is smaller over the South Asian monsoon region when compared to its surroundings. At noon and during af-

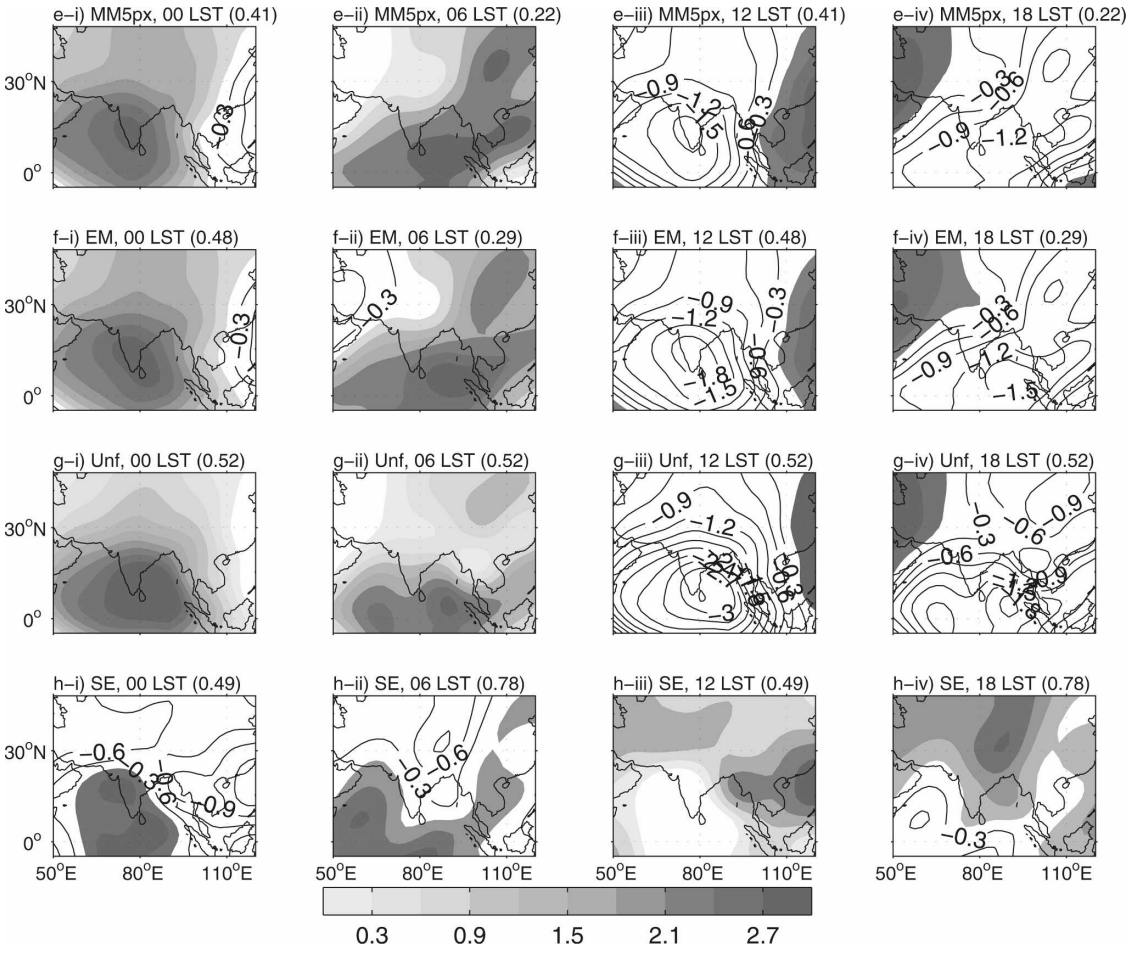

FIG. 3. (*Continued*)

ternoon hours (1200 and 1800 LST) the situation reverses. This seesaw pattern in the diurnal cycle of velocity potential over the South Asian monsoon region (10°–30°N, 70°–100°E; labeled as IN in Fig. 4) and its surroundings (5°S–45°N, 50°–120°E minus the region IN; labeled as OUT in Fig. 4) is shown in Fig. 5 during day 3 of forecasts for the break and active monsoon periods. Over the region IN during break monsoon (Fig. 5a), the ERA-40 diurnal cycle shows negative velocity potential during 0000 and 0600 LST and positive velocity potential during other half of the day. The peak of ERA-40 data is at 1200 LST. Both the ensemble mean and the unified scheme show a nearly out of phase diurnal cycle over this region compared to ERA-40. The correlation coefficients (CCs) of the time series of ensemble mean and unified scheme with the ERA-40 datasets are −0.81 and −0.75, respectively, while that for the superensemble is 0.84. During active monsoon over the region IN (Fig. 5c), the peak in the velocity potential is at 1800 LST, as opposed to 1200

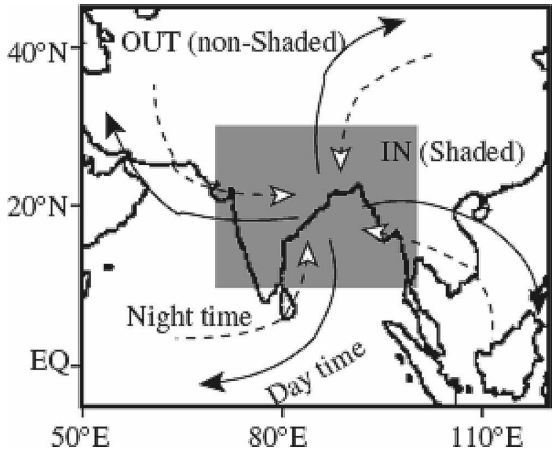

FIG. 4. Schematic of the divergent circulation at 200 hPa over the South Asian monsoon region during day (solid line) and night (dashed line) times including shaded region (IN) and nonshaded region (OUT) used in different analyses in this study.

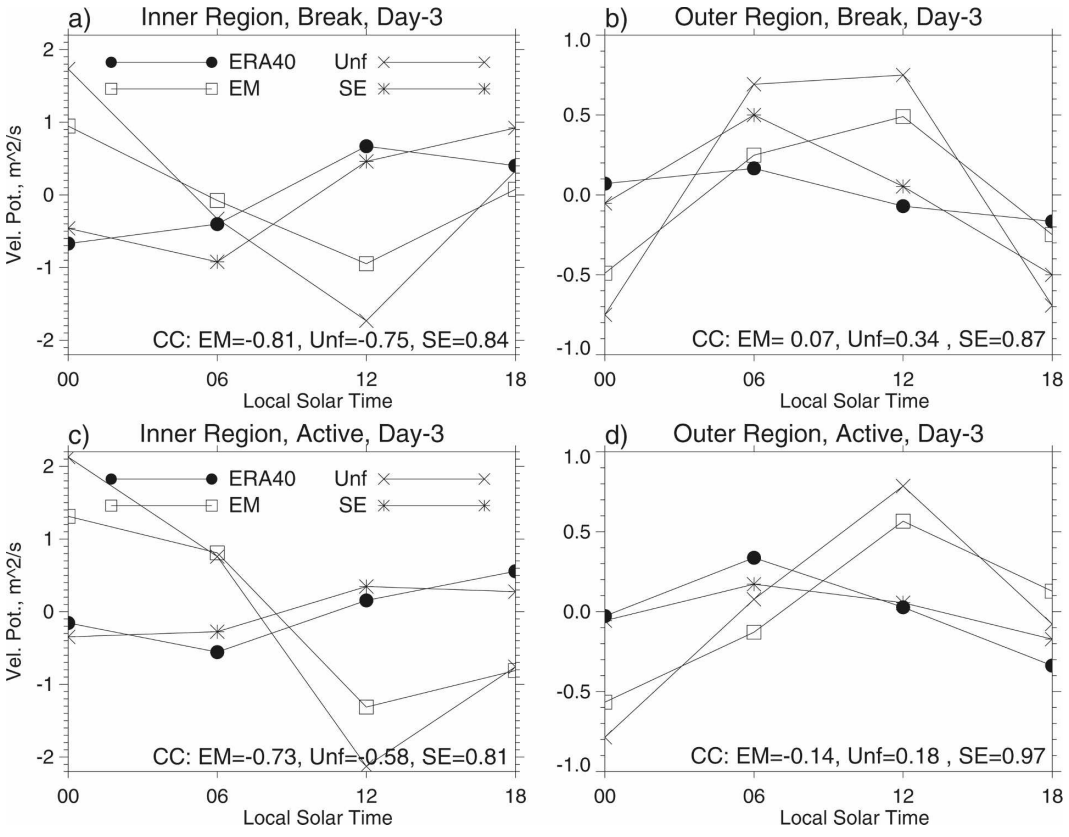

FIG. 5. The diurnal cycle of velocity potential over the South Asian monsoon region and its surroundings (regions marked as IN and OUT in Fig. 4) from ERA-40, the ensemble mean of the four member models, the unified cloud scheme, and the superensemble during day 3 of the forecasts for (a) break monsoon (23 Jul to 1 Aug 2000) and (b) active monsoon (22–31 Aug 2000): correlation coefficients of the forecasted diurnal cycles with ERA-40 indicated inside the panels.

LST in the break monsoon. This is consistent with the results shown in Figs. 2 and 3. The amplitudes of the diurnal cycle from the ensemble mean and unified scheme are much higher compared to ERA-40, and the peak appears 6 h later (CCs are −0.73, −0.58, and 0.81 for the ensemble mean, unified scheme, and superensemble, respectively).

Over the outer region (OUT; right panels of Fig. 5) a distinct peak in the ERA-40 datasets is noticed at 0600 LST during the active monsoon. However, the amplitude of the diurnal variation is much less during the break monsoon. Over this region, the member models (represented by their ensemble mean) and the unified scheme perform slightly better than over the inner region. During the break period, the ensemble mean shows higher velocity potential during 0600 and 1200 LST and lower values during 0000 and 1800 LST. The CC of the time series of the ensemble mean with ERA-40 is 0.07. The unified scheme performs better than the ensemble mean (CC = 0.34). The superensemble forecasts are very close to those of ERA-40 with a maximum at 0600 LST and minimum at 1800 LST (CC = 0.87). During the active period, both the ensemble mean and the unified scheme show peak at 1200 LST, 6 h later than in the ERA-40 dataset. It was possible to predict this phase of the diurnal cycle of velocity potential at 200 hPa by the superensemble during day 3 of the forecasts (CC = 0.97).

This shows that the seesaw pattern in the diurnal cycle of velocity potential at 200 hPa over the South Asian monsoon region and its surroundings was better predicted by the superensemble during both break and active monsoon periods. The member models and the unified scheme performed poorly over the monsoon domain, but the unified scheme did reasonably better over the surrounding regions. This high and low in velocity potential sets up a gradient that reverses its sign during the day and night hours. The corresponding circulation pattern is illustrated by the arrows in Fig. 4.

b. Diurnal cycle of horizontal winds

The diurnal cycle (at 0600 and 1800 LST for clarity) of the horizontal wind vector at 200 hPa from ERA-40, the ensemble mean of four member models, the unified scheme, and the superensemble are shown in Fig. 6 during the break monsoon period. The divergence of the horizontal wind is indicated in the background as shaded (divergent region) and contour (convergent region). Over the northern parts of India, the Tibetan Plateau, and Southeast Asia, major regions of convergence are noticed during early morning hours (Fig. 6a). Winds from the surroundings rush toward this region at late night and early morning hours. The situation reverses during 1800 LST (Fig. 6b). The convergent regions at 0600 LST become divergent regions at 1800 LST, and wind flows out of this region. For the ensemble mean there is no clear convergent region at 0600 LST over the Tibetan Plateau (Fig. 6c). A shallow convergent region is noticed over central India, far south of that of the observed. The corresponding wind pattern is also affected by this southward-shifted convergent region. The PC of the divergence field for the ensemble mean with that of ERA-40 is 0.07. The unified cloud scheme performed better than the ensemble mean in the location of the convergence (0600 LST) and divergence (1800 LST) fields (Figs. 6e,f), which are shifted slightly northward closer to the ERA-40 fields. The location of divergence and convergence over Southeast Asia is also captured by the unified scheme (PC = 0.12). The superensemble shows the best forecast of the horizontal wind vector at this level. Over the Tibetan Plateau, a major region of convergence at 0600 LST and divergence at 1800 LST is forecasted reasonably. Also, regions of divergence (convergence) over the equatorial Indian Ocean at 0600 (1800) LST are captured by the superensemble. The PC of this forecast with ERA-40 is 0.31. Note here that, although the superensemble forecast is better than other forecast products, the superensemble could not capture some of the features of the diurnal cycle of the Asian monsoon circulation.

The corresponding diurnal cycle of vector wind at 925 hPa is shown in Fig. 7. Vectors with large amplitude of diurnal variation are noticed near the coasts. This is indicative of a clear land–sea contrast at this pressure level. The amplitude of this variation is about 3–4 m s^{-1}. During daytime the land heats up faster than the ocean. This forms a thermal-low pressure that drives the sea breeze toward the land in the afternoon hours. This is evident in the ERA-40 data at 1800 LST (Fig. 7b). However, at night the land cools faster than the oceans and a land breeze blows from the land to the ocean during early morning hours (Fig. 7a). This relative warming/cooling of land and ocean during day and night hours and the corresponding diurnal cycle of wind flow is present in the forecasts from the ensemble mean, unified scheme, and superensemble (Fig. 7c–h). However, the superensemble forecasts are better compared to the other two products. This is evident in the PC of the divergent field (PCs are 0.44, 0.47, and 0.82 for the ensemble mean, unified scheme, and superensemble, respectively).

The convergence (divergence) of wind at 200 hPa during early morning (afternoon) hours (Fig. 6) and the opposite wind direction near the surface (Fig. 7) indicates a three-dimensional circulation that diurnally overturns in the spatial scale of the Asian summer monsoon. Similar circulation patterns were noticed in the active monsoon period as well (not shown). The following section presents the signature of this three-dimensional flow in the vertical velocity field.

c. Diurnal cycle of vertical velocity

The diurnal cycle of vertical pressure velocity at eight different pressure levels over the South Asian monsoon region (IN) and its surroundings (OUT) from ERA-40, the ensemble mean of the member models, the unified scheme, and the superensemble are shown in Figs. 8 and 9 during break and active monsoon periods, respectively, for day-3 forecasts. In the upper levels (200, 300, and 400 hPa) a downward motion (positive pressure velocity) is noticed over the South Asian monsoon region in the ERA-40 datasets at midnight and in the early morning hours during the break monsoon (Fig. 8). The vertical velocity is mostly upward over the surrounding region during this time. This is consistent with the convergence of winds at 200 hPa noticed in Figs. 2 and 6. At noon and during afternoon hours, upward motion prevails over the South Asian monsoon region and downward motion prevails over the surroundings in the upper levels. This is also consistent with the divergent circulation at 200 hPa during the afternoon hours noticed in Figs. 2 and 6. This characteristic of the diurnal mode of vertical pressure velocity is poorly captured by the ensemble mean and the unified scheme. Forecasts from both of these schemes are phase shifted by 6 h too late. However, the amplitude of this diurnal mode is somewhat better for the unified scheme compared to the ensemble mean. This improvement is evident in the rms errors shown inside the respective forecast panels. The rms error of the diurnal cycle is minimum for the superensemble forecasts. The superensemble successfully captured the phase and amplitude of the diurnal cycle of vertical velocity over both these regions at upper levels.

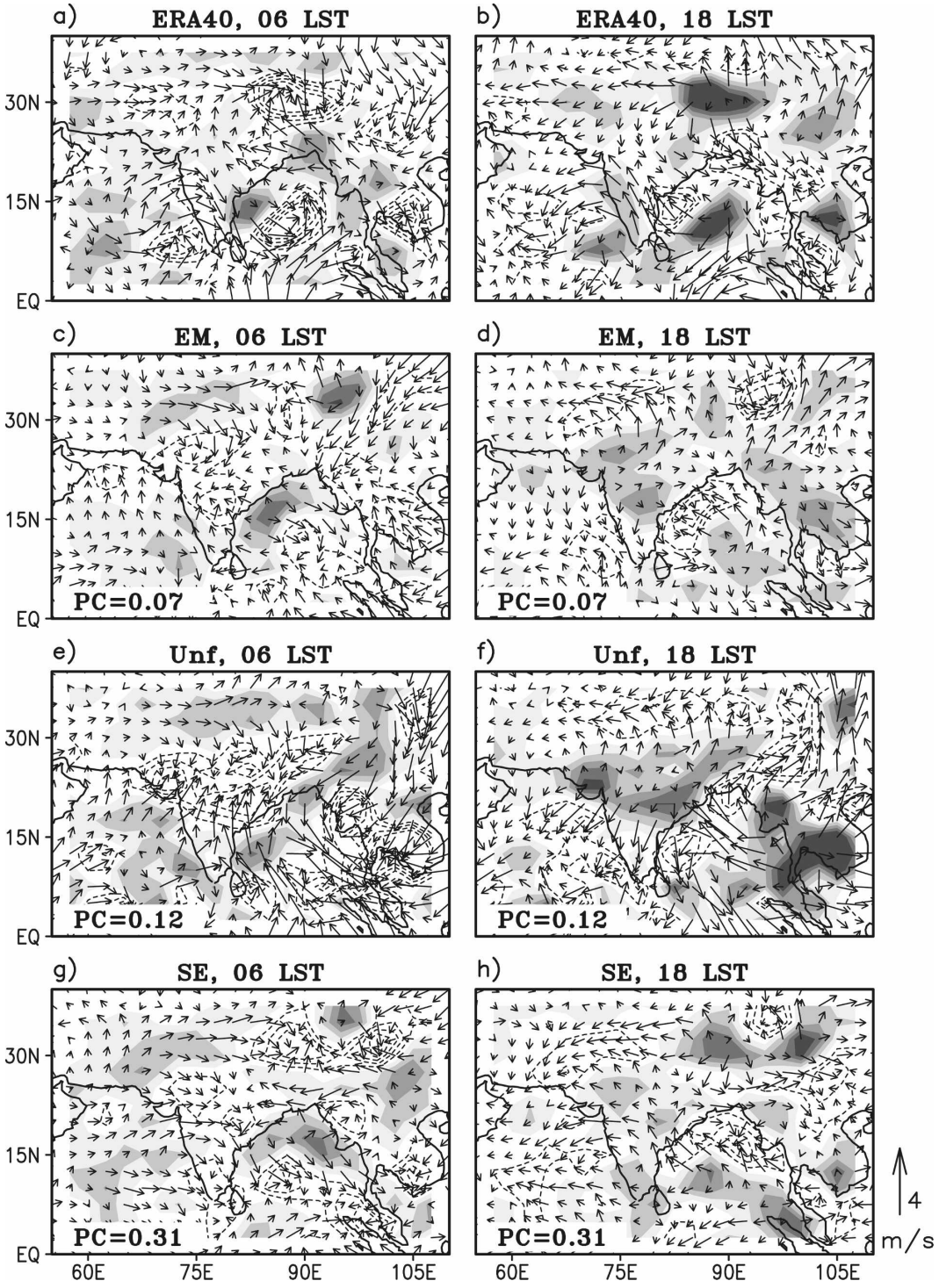

FIG. 6. The diurnal cycle of horizontal wind vector at 200 hPa from ERA-40, the ensemble mean of four member models, the unified cloud scheme, and the superensemble for day 5 of the forecasts during break monsoon (23 Jul to 1 Aug 2000): shaded (contoured) regions show locations of major divergence (convergence). Pattern correlations of the divergence of the forecast fields with ERA-40 are indicated in respective panels.

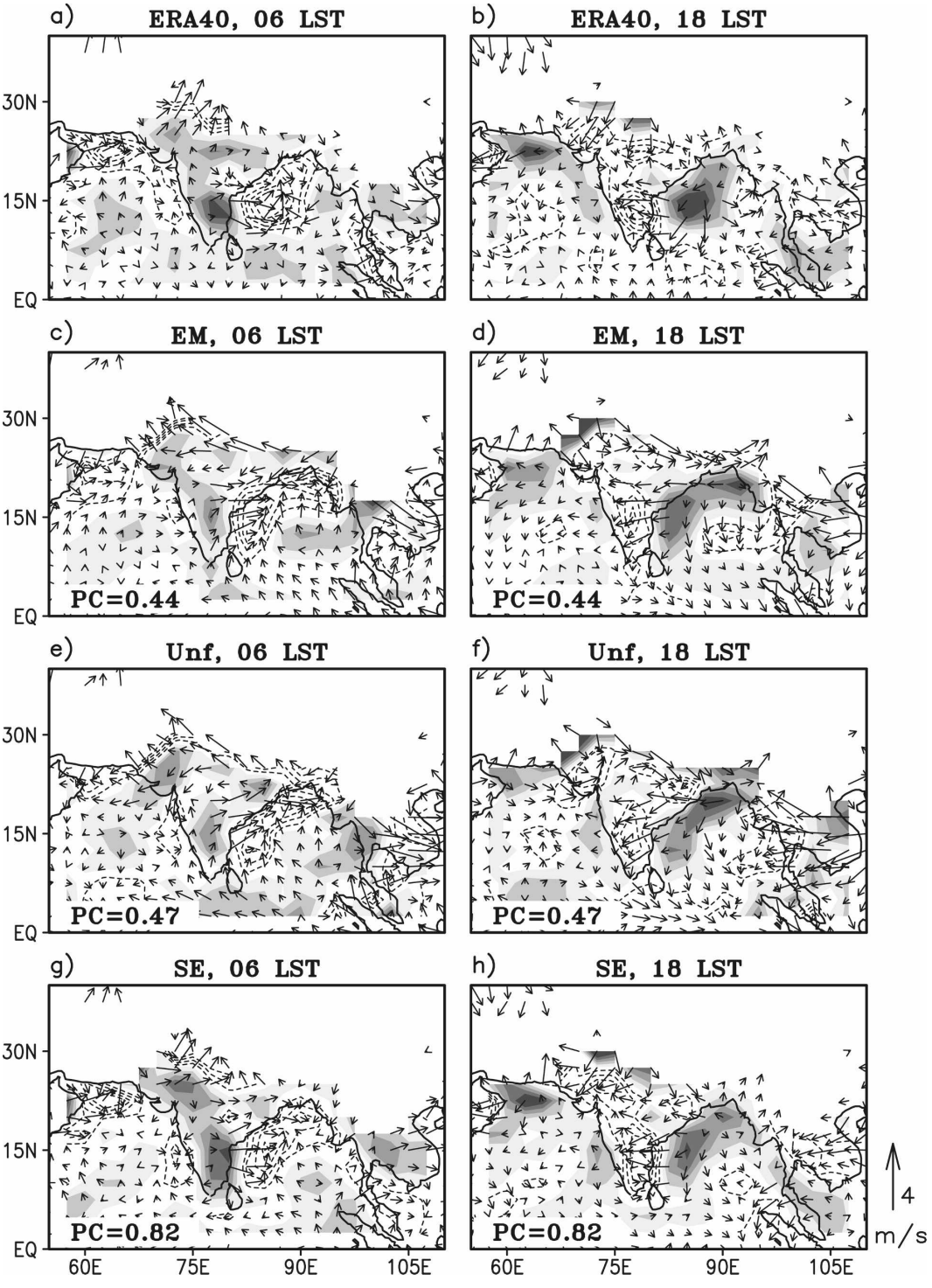

FIG. 7. As in Fig. 6 but at 925 hPa.

The diurnal cycle is not very strong at 500 hPa, although it carried the same sign of the upper levels. From Fig. 8 it is clear that this is the level of transition in the characteristics of the diurnal cycle. At 600- and 700-hPa levels over the South Asian monsoon region, upward motion is noticed at 0600 and 1200 LST and downward motion at 0000 and 1800 LST. The sign of vertical velocity is completely opposite in the outer do-

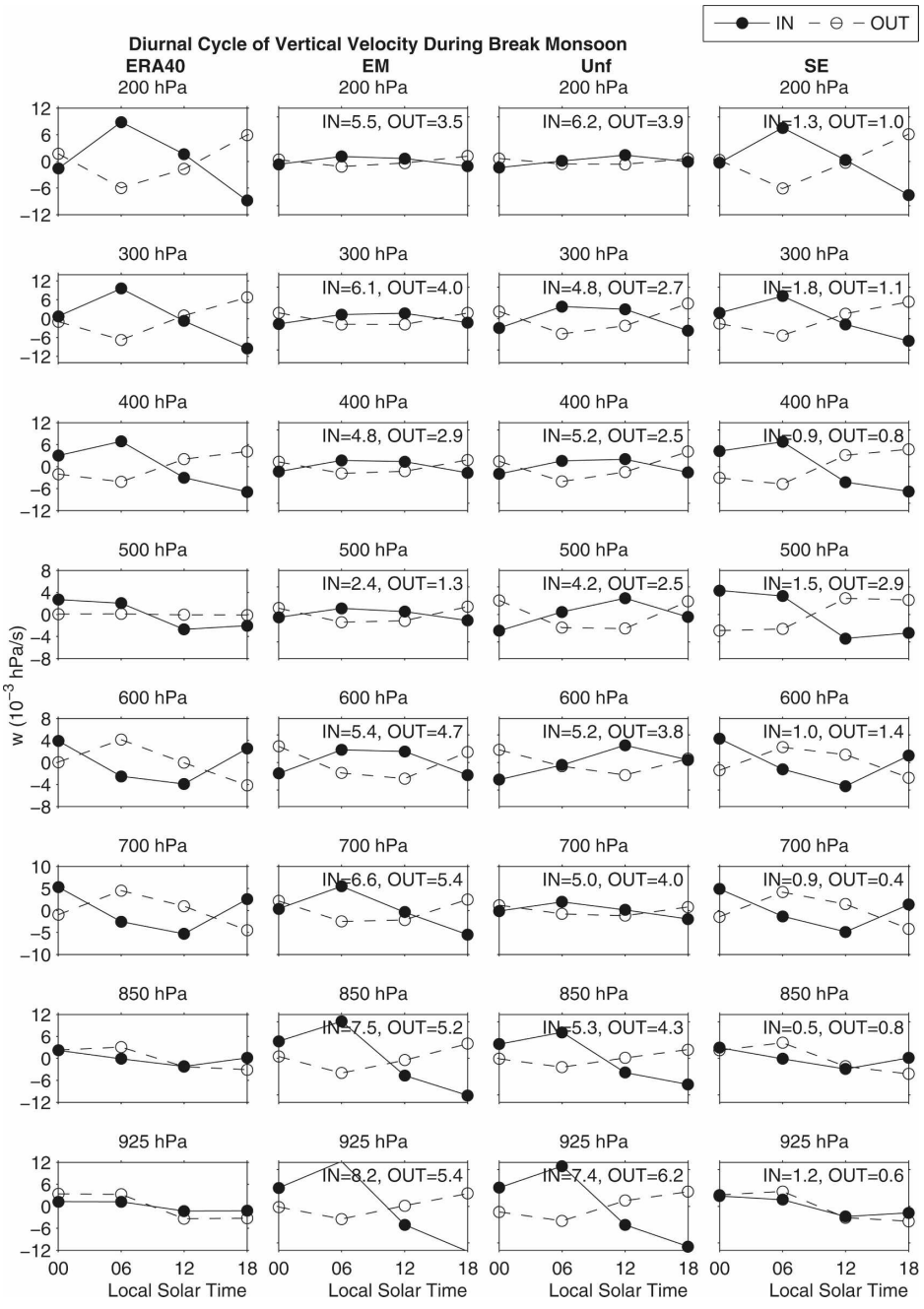

FIG. 8. The diurnal cycle of vertical pressure velocity at eight different levels over the monsoon domain (10°–30°N, 70°–100°E; indicated as IN in Fig. 4) and its surroundings (5°S–45°N, 50°–120°E; indicated as OUT in Fig. 4) during monsoon breaks: Rms errors of the forecast fields indicated inside the respective panels.

main. Both the ensemble mean and unified scheme completely missed this phase of the vertical velocity at the 600- and 700-hPa levels. The phase and amplitude of the superensemble forecasts are very close to the ERA-40 datasets.

The ERA-40 data showed a weak diurnal variation at 850- and 925-hPa levels. The phase of this variation is very similar over the South Asian monsoon region and its surroundings with downward motion at midnight and during early morning hours and upward motion at noon and during afternoon hours. The ensemble mean and the unified scheme show a large amplitude of di-

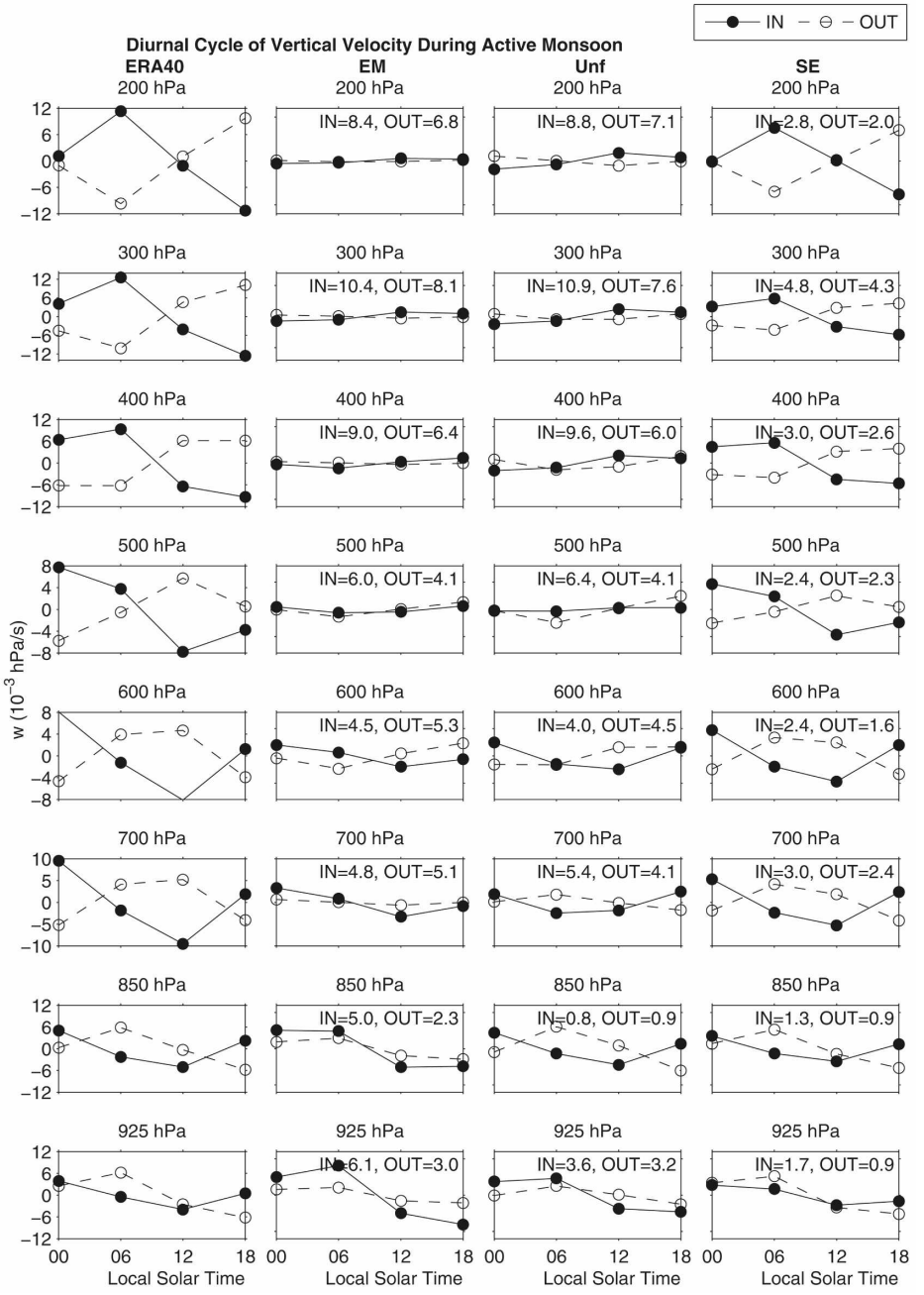

FIG. 9. As in Fig. 8 but for the active monsoon.

urnal variation at these pressure levels and had the highest rms errors. Forecasts from the superensemble are very close to that of ERA-40. Rms errors from the superensemble are almost one order of magnitude less compared to the other two forecasts.

The active monsoon shows a similar signature of the diurnal cycle of vertical pressure velocity (Fig. 9). However, the amplitude of the oscillation is higher, particularly in the middle and lower troposphere. At 925 hPa, a distinct peak of the diurnal cycle over IN is noticed at 1800–0000 LST, which is very weak during the break monsoon period. The peak is at 0600 LST over the outer region at this pressure level. The amplitude of this diurnal oscillation increases with height and reaches a maximum at 700 hPa in the ERA-40 datasets. Above 500 hPa, the peak of vertical pressure velocity occurs at 0600 LST, 6 h later compared to the lower levels. The South Asian monsoon region (IN) and its surroundings

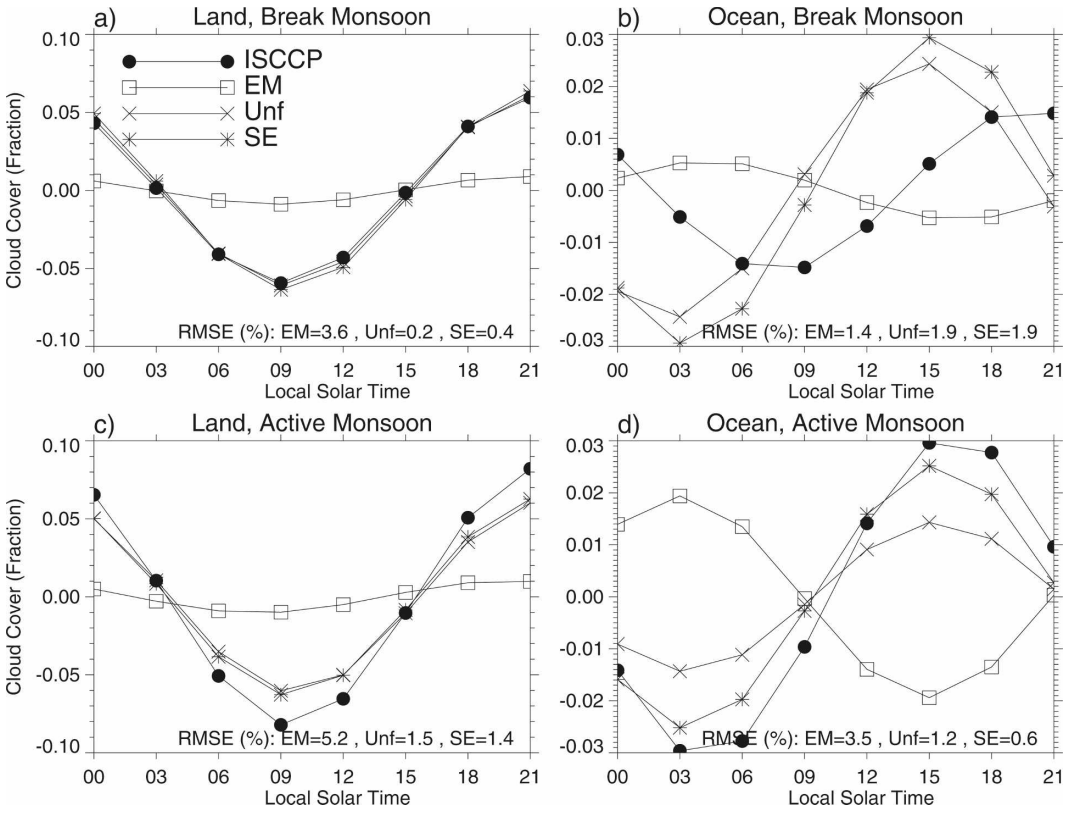

FIG. 10. The diurnal cycle of high clouds over 10°–30°N, 70°–100°E during (top) break monsoon and (bottom) active monsoon periods from ISCCP, the ensemble mean of four member models, the unified cloud scheme, and the superensemble: Rms error of the forecasts indicated inside the panels.

(OUT) are out of phase at every pressure level from the surface up to 200 hPa. Figure 9 shows that the ensemble mean and the unified scheme predicted a very weak diurnal cycle in the upper levels and a stronger diurnal cycle in the lower levels compared to the ERA-40-based estimates. The out of phase relationship between the inner and outer regions is also not captured by these simulations. As a result, the rms errors of the forecasted fields are high from these simulations. It was possible to reduce this error with use of the superensemble at all pressure levels. The superensemble could realistically capture the out of phase relationship of pressure velocity between the regions IN and OUT. The peak over the inner region during 0000 LST below 500 hPa and during 0600 LST above 400 hPa is forecasted reasonably by the superensemble. Overall, the reduction in rms errors is 2 to 3 times compared to the ensemble mean and the unified scheme.

Therefore, the three-dimensional structure of the diurnal overturning of the Asian summer monsoon is evident in the upper-level (Figs. 2, 3, and 6) and near-surface (Fig. 7) horizontal winds and in the vertical velocity fields (Fig. 8 and 9). There is a large difference (6–12 h) in phase of the diurnal cycle of vertical velocity near the surface and in the upper levels during both active and break periods. This is maintained by the out-of-phase diurnal mode in vertical velocity over the South Asian monsoon region and its surroundings.

d. Diurnal cycle of clouds and precipitation

The diurnal cycle of high clouds from ISCCP satellite-based estimates, the ensemble mean of the four models, the unified cloud scheme, and the superensemble are shown in Fig. 10 for day-5 forecasts separately over the land and ocean areas of 10°–30°N, 70°–100°E. Also shown, inside the respective forecast panels, are the rms errors of the forecasts of the total diurnal cycle in percent. Over the land parts of this region during the break monsoon (Fig. 10a), the ISCCP-based estimates show the phase of the diurnal cycle at 2100 LST with an amplitude of about 6%. The ensemble mean of the models show a very weak diurnal variation of high clouds over land. The amplitude of this variation is less than 25% of that of the ISCCP-based estimates. However, the ensemble mean of the models correctly captured the phase of the diurnal

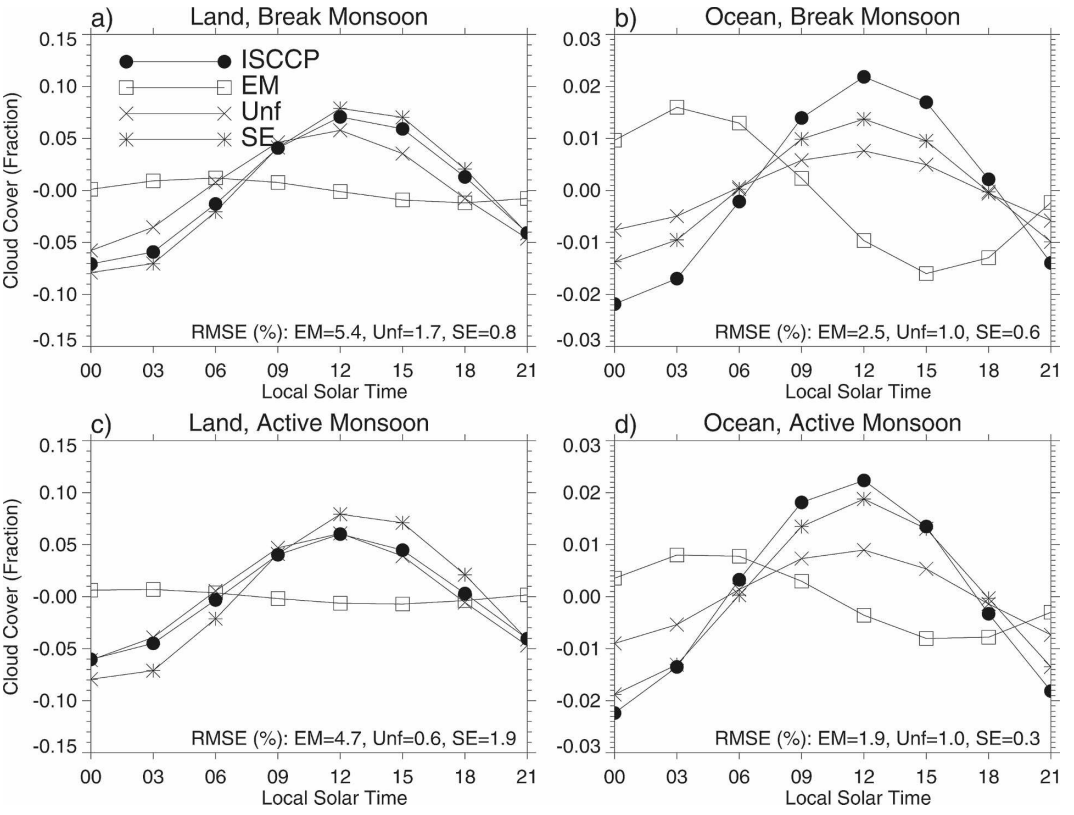

FIG. 11. As in Fig. 10 but for low clouds.

cycle. The rms error of the ensemble mean is 3.6%. On the other hand, both the unified scheme and the superensemble forecasted the phase and amplitude of the diurnal cycle reasonably well. The rms errors for these forecast schemes are 0.2% and 0.4%, respectively.

Over the ocean parts of the South Asian monsoon domain during the break period (Fig. 10b), high clouds from ISCCP datasets show the peak at 1800–2100 LST. The amplitude of this diurnal variation is about 2%, lower than that over land (6%). The unified cloud scheme and the superensemble showed phase errors of 3–6 h over this region. The rms error of the total diurnal cycle for both these forecasts is 1.9%. Although the ensemble forecast carries a lower rms error, its diurnal cycle is 180° out of phase compared to the ISCCP datasets. Comparing Figs. 10a and 10b, one can state that the ensemble mean forecasts completely missed the land–ocean contrast in amplitude of the diurnal cycle of high clouds. In the ISCCP data, land has a higher amplitude compared to over the oceans. However, the ensemble mean shows almost similar amplitude over both oceans and land.

The active period (Figs. 10c and 10d) is characterized by a higher amplitude of diurnal variation over both land and ocean. However, while the phase over land remains the same (at 2100 LST), the phase over ocean is 3–6 h earlier during the active monsoon period than in the break monsoon period. Both the unified cloud scheme and the superensemble were able to realistically capture this phase of the diurnal cycle of high clouds over land and ocean. The phase from ensemble mean forecasts is during the morning hours over both land and oceans. Moreover, over land the diurnal variation is very weak (amplitude ~1% compared to 8% in the ISCCP estimates). The rms errors of the forecasts were reduced by the unified scheme and the superensemble.

The diurnal cycle of low clouds over land parts of the South Asian monsoon domain, on the other hand, had a phase at 1200 LST during both break and active periods (Figs. 11a and 11c), 9 h earlier than the peak in high clouds (Figs. 10a and 10c). The amplitude of the diurnal cycle is about 7%. The ensemble mean of the four cloud schemes failed to forecast this phase and amplitude of the diurnal cycle of low clouds during day 5. The ensemble mean forecasts showed a weak diurnal variation with amplitude of around 1% and phase at 0600 LST. It was possible to correct this huge error in the member models with use of the unified cloud scheme and the multimodel superensemble. The rms

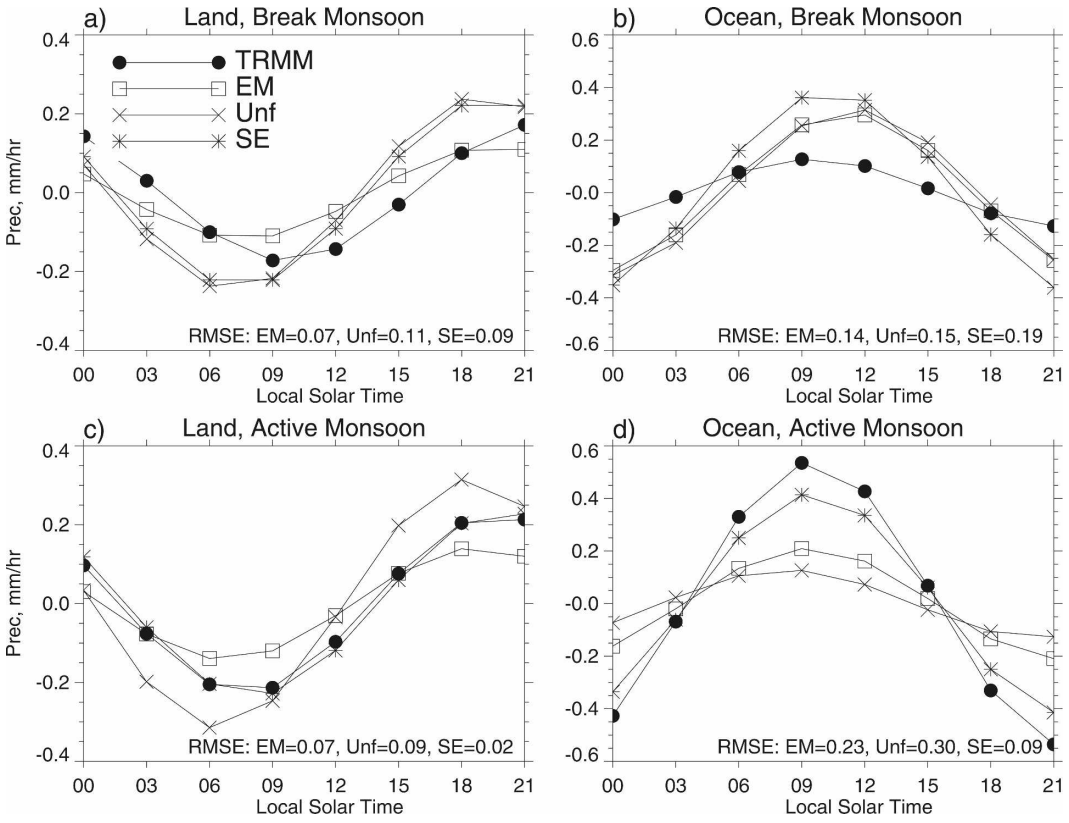

FIG. 12. As in Fig. 10 but for precipitation.

error of the entire diurnal cycle were reduced to below 2% by these products as opposed to more than 4.5% in the ensemble mean forecasts.

Low clouds over the ocean parts of the South Asian monsoon region also showed a peak at 1200 LST during both break and active periods (Figs. 11b and 11d). When compared to the phase of high clouds, this is about 9 h earlier during the break period and 3 h earlier during the active period. However, the ensemble mean of the models showed the peak of high and low clouds at the same time. The unified scheme and the superensemble correctly predicted both phase and amplitude of the diurnal variation of low cloud over the ocean. The rms error of the total diurnal cycle from the ensemble mean, unified scheme, and superensemble forecasts are, respectively, 2.5%, 1.0%, and 0.6% during the monsoon break, and 1.9%, 1.0%, and 0.3% during the active monsoon period.

The diurnal cycle of precipitation over South Asia (10°–30°N, 70°–100°E) during the break and active periods is shown in Fig. 12 from TRMM-based estimates, the ensemble mean of the member models, the unified scheme, and the superensemble. Over the land parts, TRMM data shows a peak at around 2100 LST during the break period and at 1800–2100 LST during the active period. The phase of this variation is captured by the ensemble mean, albeit an underestimation in the amplitude of diurnal variation during both break and active periods. The unified cloud scheme slightly overestimates the amplitude during both break and active periods. The superensemble forecasts were better than the ensemble mean and the unified scheme, especially when monsoon is active over this region.

Over the ocean parts, the difference in diurnal amplitude for the active and break monsoon is large. While the diurnal cycle of the monsoon break shows an amplitude below 0.2 mm h^{-1}, it is more than 0.5 mm h^{-1} during the active monsoon. However, the phase during both of these extreme precipitation periods is at 0900 LST. All three forecasts overestimate the amplitude during the monsoon break and underestimate it during the active monsoon. However, the superensemble forecast is closer to the TRMM datasets, particularly during the active season. Note that the peak of precipitation over the ocean occurred about 6–9 h earlier than the high clouds, which is in accordance with the observation by Tian et al. (2004). Owing to a large phase error for the ensemble mean in forecasting the diurnal cycle of high clouds over ocean, the aforementioned phase difference between precipitation and high

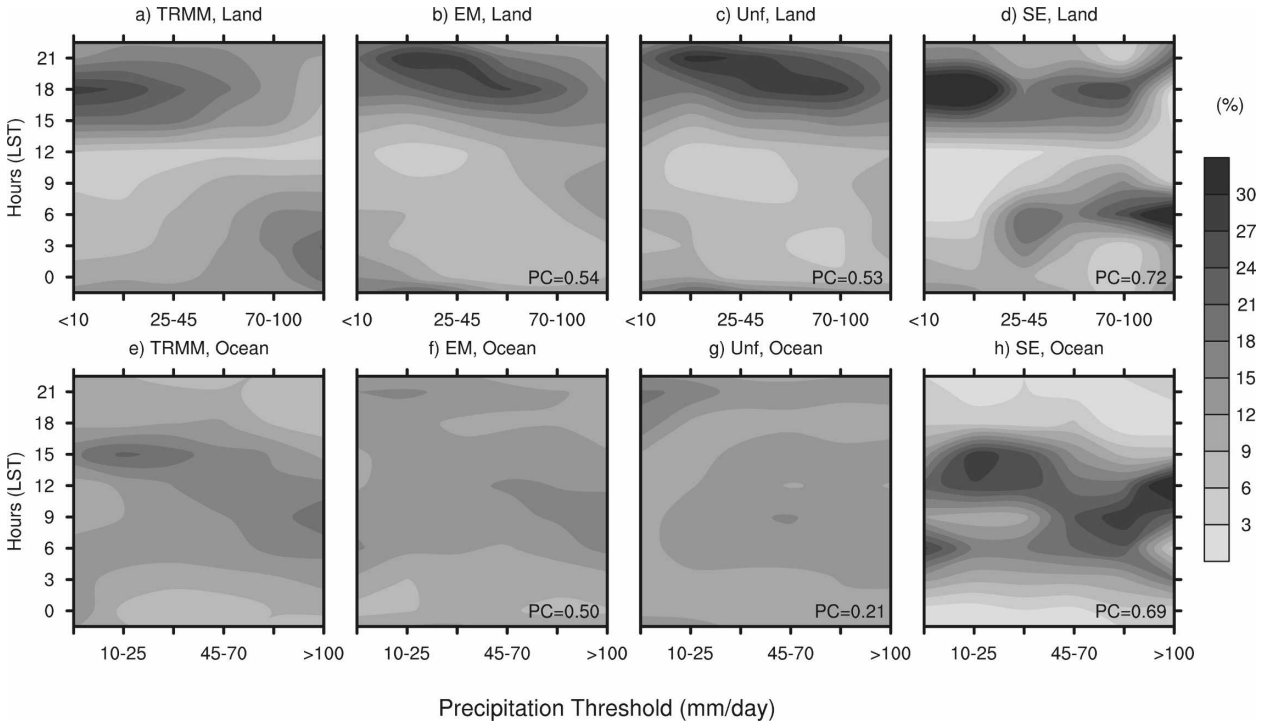

FIG. 13. Relative occurrences (%) of the peak of the diurnal cycle of precipitation during different hours of a day for various precipitation ranges during 20 Jul to 5 Sep 2000 for day 5 of the forecasts from TRMM, the ensemble mean, the unified scheme, and the superensemble over the land and ocean areas of 10°–30°N, 70°–100°E: PC of the forecast fields with the observed counterpart indicated inside the respective panels.

clouds is absent in the ensemble mean forecasts. Both the unified cloud scheme and the superensemble are consistent in capturing this difference in the phase of the diurnal cycle precipitation and high clouds.

e. Relative distribution of diurnal phase of precipitation during a day

Relative occurrences (in %) of the phase of diurnal precipitation during different hours of a day at various precipitation ranges over the land and ocean areas of the South Asian monsoon region for the entire 47 days of day 5 forecasts (20 July–5 September 2000) are shown in Fig. 13. At first, the hour corresponding to the peak of precipitation during each day (i.e., diurnal phase) was calculated and grouped into different bins according to the total precipitation on that day. The bin intervals were <10, 10–25, 25–45, 45–70, 70–100, and >100 mm day^{-1}. Now, the relative occurrences of peak hour of precipitation were obtained by dividing the number of days at every 3 h by the total number of days at that bin. We have included all 47 days of the forecasts (instead of two separate 10-day periods for the break and active monsoon periods) to obtain a complete picture at all precipitation ranges. The results show that over land for the TRMM dataset the peak in precipitation occurred mainly during afternoon hours (1500–2100 LST) when total precipitation on that day is below 70 mm. However, for precipitation exceeding 70 mm day^{-1}, the peak in precipitation shifts to late night/early morning hours (0000–0600 LST). The ensemble mean and the unified scheme showed a delayed phase in occurrences (by about 3 h) for both light and heavy precipitation. The superensemble showed correct phase for low to moderate precipitation (<25 mm day^{-1}). However, two distinctly different preferred times of the phase are forecasted for moderate to heavy precipitation ranges (25–100 mm day^{-1}), one being in the afternoon hours and another during early morning hours (0300–0600 LST). While the afternoon hour peak agreed with the TRMM data, the TRMM does not show a very clear peak in the late night hours for this range of precipitation. For very heavy precipitation (>100 mm day^{-1}), the observed (TRMM) peak during 0000–0600 h is reasonably captured by the superensemble. The overall pattern of the superensemble forecasts (PC = 0.72) improved compared to the ensemble mean (PC = 0.54) and the unified schemes (PC = 0.53).

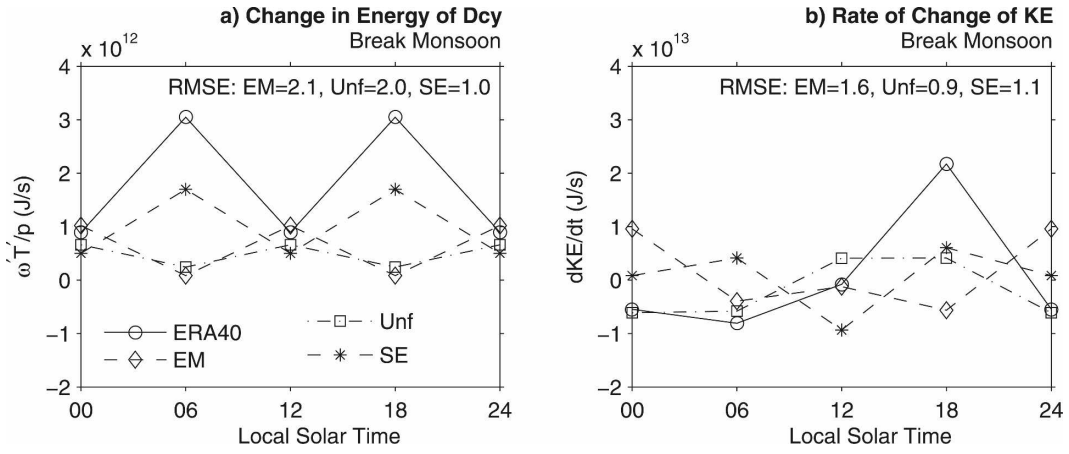

FIG. 14. Contribution of the energy of the diurnal cycle to the total kinetic energy over 10°–30°N, 70°–100°E during the break monsoon period from ERA-40, the ensemble mean of the member models, the unified scheme, and the superensemble: rms error of the forecast fields are indicated inside the panels.

Using a Student's *t* test, it was found that this improvement is significant at the 95% level when compared to the ensemble mean.

Over the ocean parts of the South Asian monsoon domain, in the TRMM datasets, the preferred phase of the diurnal precipitation is at 1200–1500 LST for low to moderate precipitation and in the early morning hours for heavy precipitation (Fig. 13e). However, these peaks were not as distinct as is noticed over land. This suggests that over oceans the chance of peak precipitation at various thresholds is distributed more evenly during all hours of the day. The ensemble mean and the unified schemes could not forecast these phases at various thresholds (PCs are 0.50 and 0.21, respectively). The peaks were more distinct for the superensemble forecasts, but were at correct hours for all precipitation thresholds. The PC of the forecast is improved for the superensemble (0.69) compared to the other two products. Similar to over the land region, this improvement in the forecasted PC is significant at the 95% level compared to the ensemble mean.

f. Contribution of the diurnal mode to the kinetic energy of the monsoon circulation

Figure 14a illustrates the contribution to the generation of kinetic energy from the diurnal mode during the break monsoon period. Here these results are tropospheric integrals from the surface to the 100-hPa level and cover the monsoon domain between 10° and 30°N, 70° and 100°E. The units are joules per second. These are composites over a 10-day period, 23 July–1 August 2000 from ERA-40 and day 5 of the forecasts from the ensemble mean, the unified scheme, and the superensemble. The important result is a net positive contribution for the integral

$$E_{\mathrm{dcy}} = -R \int_m \frac{\omega' T'}{P}\, dm \tag{7}$$

for the diurnal mode, where R is gas constant for air, P is pressure, and ω' and T' are the diurnal component of vertical pressure velocity and air temperature: $\int_m [\,]\, dm$ represents the mass-weighted integral

$$\int_m [\,]\, dm = \frac{1}{g} \int_P \int_y \int_x [\,]\, dx\, dy\, dP, \tag{8}$$

where g is acceleration due to gravity, x and y represent longitude and latitude directions respectively, and P is the pressure. This positive contribution of the diurnal mode is clearly seen in the observed estimates and the superensemble forecasts. The ensemble mean and the unified scheme fail to capture this feature. The important implications of this result are as follows: Each day this diurnal mode is providing energy for driving the monsoon via the thermally direct diurnal vertical circulations. The daily averaged magnitude of that energy transfer for the diurnal to the monsoon scale is of the order of 10^{12} J s^{-1}. Having the same positive sign every day makes this effect quite large accumulatively over a monsoon season.

Figure 14b illustrates the contributions to the local change of total kinetic energy for the same period for ERA-40, the ensemble mean, the unified scheme, and the superensemble over the same monsoon domain. This is expressed by

$$\dot{K} = \int_m \frac{\partial K}{\partial t}\, dm, \tag{9}$$

where K is the kinetic energy. These results for a 10-day average depend strongly on the prevailing monsoon

phenomenology of that period. This change of total kinetic energy is of the order of 10^{13} J s^{-1} and is one order of magnitude larger than the diurnal change. This change, on an hour by hour basis, shows a net positive growth of total kinetic energy from the observed estimates (7.3×10^{13} J s^{-1}) and the multimodel superensemble (1.7×10^{13} J s^{-1}). The ensemble mean (-1.2×10^{13} J s^{-1}) and the unified model (-3.7×10^{13} J s^{-1}) do not show a positive contribution during this period. In terms of rms error, both the unified scheme and the superensemble showed higher skills compared to the ensemble mean forecasts. Note that the change in energy of the diurnal cycle over the Asian monsoon region is of the order of 10^{12} J s^{-1}, and rate of change of kinetic energy over the same domain is of the order of 10^{13} J s^{-1}. Therefore, it appears that the diurnal change contributes roughly 10% to the total change of kinetic energy of the Asian summer monsoon. Similar results were found during the active monsoon period (not shown). Because of the steady contribution of the diurnal change this is an important aspect of the monsoon.

7. Conclusions

The major finding of this study is that a pronounced diurnal mode of the three-dimensional tropospheric circulation over the Asian monsoon region exists. Intense precipitation and upward velocity is noticed over this monsoon domain at noon and during the afternoon hours. This leads to a divergent circulation in the upper troposphere and outflow from this region to its surroundings. This is best seen in the 200-hPa velocity potential (Krishnamurti and Kishtawal 2000).

The available 6-hourly ERA-40 datasets show that this divergent circulation peaks at 1200 LST during monsoon breaks and at 1800 LST during active monsoon periods. The diurnal cycle of the pressure velocity in the upper troposphere is upward (downward) in the afternoon (early morning) hours above the 500-hPa level. In the lower troposphere, this phase of the diurnal cycle occurs 6 h earlier than in the upper levels. Moreover, the ascending motion is more intense, especially at the middle and lower troposphere during the active monsoon period than during monsoon breaks. In the surrounding regions, on the other hand, downward motion is evident during daytime. Another component of this three-dimensional circulation is the wind flow toward the South Asian land from the nearby oceans at noon and during the afternoon hours near the surface. At midnight and during the early morning hours this scenario completely reverses. ISCCP satellite-based observations at 3-h intervals show that, over land parts of the Asian monsoon region, the peak in the diurnal cycle of high clouds is at 2100 LST during both break and active phases. However, the amplitude is about 2.5% higher during the active period than during the break period. Over ocean parts, the phase of the diurnal cycle of high clouds is at 1800–2100 LST during break monsoon and 1500–1800 LST during active monsoon. Similar to that over land, the amplitude is higher during the active period as compared to the break period of monsoon. The diurnal cycle of low clouds does not show any major difference in phase and amplitude during active and break periods. TRMM satellite-based 3-hourly precipitation estimates over land parts of the monsoon domain peak at 2100 LST during the break period and 1800–2100 LST during the active period. Over the ocean part, a weak peak is present in the morning hours during the monsoon break and a sharp peak is noticed at 0900 LST during the active monsoon period. Overall, moderate to heavy precipitation (10–100 mm day^{-1}) usually peaks in the afternoon hours (1800 LST) and very heavy precipitation (>100 mm day^{-1}) peaks in the early morning hours (0300 LST; about 9 h later) over land. Over oceans, very heavy precipitation occurs about 6 h earlier compared to moderate precipitation.

This study demonstrates that global GSMs carry a signature of this pronounced diurnal mode over the Asian monsoon region. However, the location and phase of the diurnal component of the 200-hPa velocity potential was completely missed by all four member models and their ensemble mean, especially over the core monsoon domain. The models performed somewhat better over the surrounding regions. The ensemble mean of the member models had large phase and amplitude errors in forecasting the diurnal cycle of vertical velocity over the core monsoon domain and its surroundings during both active and break monsoon periods.

With the use of a multimodel superensemble, it was possible to substantially reduce the forecast errors for the phase and amplitude of this three-dimensional diurnal mode of the Asian summer monsoon out to five days in advance. This was due to the assignment of differential weights to the member models based on their past performance. The superensemble showed the highest PC for the 200-hPa velocity potential during day 3 of the forecasts during active and break monsoon periods. The phase and amplitude of vertical velocity over both the core monsoon region and its surroundings were correctly predicted through day 5 of the forecasts by the multimodel superensemble.

This study also used a statistical–physical-based unified cloud parameterization scheme (Chakraborty et al. 2007) for forecasting this large-scale diurnal circulation.

This scheme used the concept of the superensemble to combine the forecasts of four member cloud schemes inside a single model. The unified cloud scheme showed higher skill than the member models in forecasting the diurnal cycle of clouds and precipitation over this region. The main advantage of a unified model is that it improves the forecast skill of a single model. Moreover, the unified model has potential to improve the forecast of other parameters through a feedback mechanism. Nevertheless, using a single model for forecasting is computationally less expensive than running a suite of multimodels.

We have shown that this diurnal mode has a direct implication to the energetics of the Asian summer monsoon. Calculations show that, on average, 10% of the rate of change of the total kinetic energy of the monsoon on a daily scale is supplied by this diurnal mode. Therefore, a better prediction of diurnal circulation could improve forecast skill of the summer monsoon. It was found that the multimodel superensemble had the highest skill in forecasting this estimated energy exchange from the diurnal mode to the total monsoonal circulation.

This study shows that a multimodel superensemble can be used to predict the diurnal mode of the Asian monsoon circulation out to five days in advance with reasonably high skill for both active and break monsoon periods. The multimodel superensemble also performs best in predicting the diurnal variation of high clouds and precipitation over both land and ocean in the South Asian region. A new unified cloud parameterization scheme did not do well for the prediction of the divergent circulation but showed a relatively high skill in predicting the diurnal cycle of clouds and precipitation. A combination of a different unified scheme (e.g., for clouds, cumulus convection, PBL) in a single model may be required to reduce forecasting errors of the diurnal circulation and other parameters within a single model.

Acknowledgments. We gratefully acknowledge ECMWF for providing the initial conditions for model simulations and ERA-40 datasets for verification purposes. ISCCP cloud data were taken from NASA Langley Research Center's ASDC Web site. This study is supported by NSF Grant ATM-0491618, NASA Grants NAGS-13563 and NNG05GH81G, and NOAA Grant NA16GP1365.

REFERENCES

Bergman, J. W., and M. L. Salby, 1997: The role of cloud diurnal variations in the time-mean energy budget. *J. Climate,* **10,** 1114–1124.

Chakraborty, A., and T. N. Krishnamurti, 2006: Improved seasonal climate forecasts of the South Asian summer monsoon using a suite of 13 coupled ocean–atmosphere models. *Mon. Wea. Rev.,* **134,** 1697–1721.

——, ——, and C. Gnanaseelan, 2007: Prediction of the diurnal cycle using a multimodel superensemble. Part II: Clouds. *Mon. Wea. Rev.,* **135,** 4097–4116.

Dai, A., 2001: Global precipitation and thunderstorm frequencies. Part II: Diurnal variations. *J. Climate,* **14,** 1112–1128.

——, and C. Deser, 1999: Diurnal and semidiurnal variations in global surface wind and divergence fields. *J. Geophys. Res.,* **104,** 31 109–31 126.

——, and K. E. Trenberth, 2004: The diurnal cycle and its depiction in the Community Climate System Model. *J. Climate,* **17,** 930–951.

Janowiak, J. E., V. E. Kousky, and R. J. Joyce, 2005: Diurnal cycle of precipitation determined from the CMORPH high spatial and temporal resolution global precipitation analysis. *J. Geophys. Res.,* **110,** D23105, doi:10.1029/2005JD006156.

Krishnamurti, T. N., and C. M. Kishtawal, 2000: A pronounced continental-scale diurnal mode of the Asian summer monsoon. *Mon. Wea. Rev.,* **128,** 462–472.

——, and J. Sanjay, 2003: A new approach to the cumulus parameterization issue. *Tellus,* **55,** 275–300.

——, C. M. Kishtawal, T. E. LaRow, D. R. Bachiochi, Z. Zhang, C. E. Williford, S. Gadgil, and S. Surendran, 1999: Improved weather and seasonal climate forecasts from multimodel superensemble. *Science,* **285,** 1548–1550.

——, ——, D. W. Shin, and C. E. Williford, 2000: Multimodel superensemble forecasts for weather and seasonal climate. *J. Climate,* **13,** 4196–4216.

——, and Coauthors, 2003: Improved skill for the anomaly correlation of geopotential heights at 500 hPa. *Mon. Wea. Rev.,* **131,** 1082–1102.

——, C. Gnanaseelan, and A. Chakraborty, 2007: Prediction of the diurnal cycle using a multimodel superensemble. Part I: Precipitation. *Mon. Wea. Rev.,* **135,** 3613–3632.

——, ——, A. K. Mishra, and A. Chakraborty, 2008: Improved forecasts of the diurnal cycle in the tropics using multiple global models. Part I: Precipitation. *J. Climate,* **21,** 4029–4043.

Kummerow, C., and Coauthors, 2000: The status of the Tropical Rainfall Measuring Mission (TRMM) after two years in orbit. *J. Appl. Meteor.,* **39,** 1965–1982.

Mishra, A. K., and T. N. Krishnamurti, 2007: Current status of multimodel superensemble and operational NWP forecast of the Indian summer monsoon. *J. Earth Syst. Sci.,* **116,** 369–384.

Pleim, J. E., and A. Xiu, 1995: Development and testing of a surface flux and planetary boundary layer model for application in mesoscale models. *J. Appl. Meteor.,* **34,** 16–32.

Randall, D. A., Harshvardhan, and D. A. Dazlich, 1991: Diurnal variability of the hydrologic cycle in a general circulation model. *J. Atmos. Sci.,* **48,** 40–62.

Reynolds, R. W., and T. M. Smith, 1994: Improved global sea surface temperature analysis using optimum interpolation. *J. Climate,* **7,** 929–948.

Rossow, W. B., and R. A. Schiffer, 1999: Advances in understanding clouds from ISCCP. *Bull. Amer. Meteor. Soc.,* **80,** 2261–2287.

——, A. W. Walker, and L. C. Garder, 1993: Comparison of ISCCP and other cloud amounts. *J. Climate,* **6,** 2394–2418.

Rozendaal, M. A., C. B. Leovy, and S. A. Klein, 1995: An observational study of diurnal variations of marine stratiform cloud. *J. Climate,* **8,** 1795–1809.

Shin, K.-S., G. R. North, Y.-S. Ahn, and P. A. Arkin, 1990: Time scales and variability of area-averaged tropical oceanic rainfall. *Mon. Wea. Rev.,* **118,** 1507–1516.

Slingo, J. M., 1987: The development and verification of a cloud prediction scheme for the ECMWF model. *Quart. J. Roy. Meteor. Soc.,* **113,** 899–927.

Stefanova, L., and T. N. Krishnamurti, 2002: Interpretation of seasonal climate forecast using Brier skill score, FSU superensemble, and the AMIP-I dataset. *J. Climate,* **15,** 537–544.

Sundqvist, H., 1978: A parameterization scheme for nonconvective condensation including prediction of cloud water content. *Quart. J. Roy. Meteor. Soc.,* **104,** 677–690.

——, E. Berge, and J. E. Kristjnsson, 1989: Condensation and cloud studies with a mesoscale numerical weather prediction model. *Mon. Wea. Rev.,* **117,** 1641–1657.

Tian, B., B. J. Soden, and X. Wu, 2004: Diurnal cycle of convection, clouds, and water vapor in the tropical upper troposphere: Satellites versus a general circulation model. *J. Geophys. Res.,* **109,** D10101, doi:10.1029/2003JD004117.

Trenberth, K. E., A. Dai, R. M. Rasmussen, and D. B. Parsons, 2003: The changing character of precipitation. *Bull. Amer. Meteor. Soc.,* **84,** 1205–1217.

Yang, G.-Y., and J. Slingo, 2001: The diurnal cycle in the tropics. *Mon. Wea. Rev.,* **129,** 784–801.

Yang, S., and E. A. Smith, 2006: Mechanisms for diurnal variability of global tropical rainfall observed from TRMM. *J. Climate,* **19,** 5190–5226.